Colloid Polym Sci (2006) 285: 1–9
DOI 10.1007/s00396-006-1526-3

ORIGINAL CONTRIBUTION

Tongwen Wang
Ozlem Sel
Igor Djerdj
Bernd Smarsly

Preparation of a large Mesoporous CeO_2 with crystalline walls using PMMA colloidal crystal templates

Received: 28 March 2006
Accepted: 30 May 2006
Published online: 31 August 2006

T. Wang · O. Sel · I. Djerdj ·
B. Smarsly (✉)
Max Planck Institute of Colloids and Interfaces, Research Campus Golm,
14424 Potsdam, Germany
e-mail: smarsly@mpikg-golm.mpg.de
Tel.: +49-331-5679509
Fax: +49-331-5679502

T. Wang
Department of Chemistry,
Yunnan Normal University,
Kunming, 650092,
People's Republic of China

I. Djerdj
Department of Physics,
Faculty of Science,
University of Zagreb,
Bijenicka 32,
P.O. Box 331, 10002 Zagreb, Croatia

Abstract Inverse opals of crystalline CeO_2 were synthesized by using close-packed poly(methyl methacrylate) (PMMA) latex spheres of various sizes as templates, resulting in pore sizes, which could be scaled down even to the mesopore region (30–40 nm). The latex spheres were synthesized by emulsion polymerization, and the PMMA particle size could be substantially decreased by addition of sodium dodecyl sulfate (SDS) as surfactant. Owing to the larger pore wall thickness, the CeO_2 with large mesopores preserves an intact porosity to higher temperatures than previously reported mesoporous CeO_2 obtained from surfactant templates. The porosity and crystallinity were studied by microscopic techniques, wide angle X-ray diffraction (XRD), N_2 sorption, and Hg porosimetry. The evolution of crystallinity (crystallite size and lattice parameters) was determined for different annealing temperatures by means of Rietveld refinements of the XRD data. Thereby, our study allowed getting general insights into the crystallization behavior of sol–gel derived porous CeO_2 frameworks.

Keywords CeO_2 · Large mesostructure · Inverse opals · PMMA · Colloidal crystals

Introduction

Cerium oxide has attracted intense interest due to its high potential applications such as supports for catalytic processes, high temperature ceramics, for promotion of water gas shift and reforming reaction, noble metal dispersion, and solid oxide fuel cells, etc. [1–6]. One of the most important properties of ceria is the ability to store and release oxygen, which is widely used as a key component of three-way catalysts for the elimination of toxic exhaust gases in automobiles [5]. Thus, for such applications, it is desirable to prepare ceria materials with enhanced textural, thermal properties, and high surface area, in particular in the form of mesoporous frameworks. In literature, various strategies have been described to fabricate mesoporous CeO_2, such as a hybrid organic/inorganic route [7] and a careful control of reaction conditions and calcination regimes [8]. However, so far, only moderate success was achieved in the goal for well-defined pore structures of crystalline CeO_2 with good thermal stability. In these previous synthesizes, smaller molecular templates were used such as cetyltrimethylam-

monium bromide (CTAB) [7] or hexadecylamine [8], and the crystallization of CeO_2 pore walls was usually accompanied by immense shrinkage of the mesostructure and eventually followed by its collapsing at higher temperatures owing to the growth of CeO_2 nanocrystals. The mesostructural collapse in the aforementioned syntheses can be attributed to the geometric incompatibility of the primary CeO_2 nanocrystal size and the mesopore size (usually only ca. 3 nm in previous studies) determined by the template. Recently, important progress was reported on the fabrication of mesoporous crystalline ceria, including our recent work, showing the preparation of thin films of well-defined mesoporous structures (with spherical pores of ca. 14 nm in size) of pure crystalline CeO_2 using a novel PHB–PEO block copolymer as template and employing the "evaporation-induced self-assembly" (EISA) [9, 10]. Another improvement in this field is the preparation of a well-ordered mesopore structure starting from preformed nanoparticles of CeO_2 of strictly uniform size. The synthesis involves self-assembly of these 5-nm CeO_2 pretreated nanoparticles in the presence of a block copolymer as structure directing agent [11, 12].

In spite of the recent advances in the preparation of mesostructured CeO_2, it is still a challenge to fabricate well-defined crystalline mesoporous CeO_2 by a straightforward templating method due to the special crystallization behavior of CeO_2. It was found that sol–gel derived CeO_2 starts crystallizing already at relatively low temperatures (200 °C) from relatively small initial nanocrystals (ca. 2 nm) [9, 10], which grow linearly with increasing heat-treatment temperature. This continuous nanoparticle growth leads to the collapse of porosity approximately at the point, when the nanoparticle size exceeds the pore size. Even the aforementioned use of improved block copolymers or starting from preformed nanoparticles could not solve this problem because, also in these cases, mesostructural breakdown occurred at higher temperature. Therefore, it appears that the intricate crystallization behavior makes it conceptually impossible to obtain crystalline CeO_2 with a stable mesopore structure and pores below ca. 20 nm in size beyond ca. 400 °C, if surfactants are used. It has to be noted that the maximum size of block copolymer micelles, which can be used for sol–gel templating, is ca. 50 nm. However, the usage of such large block copolymers imposes further difficulties (reduced mobility in the sol–gel solution), and they also have to be synthesized by elaborate techniques (usually anionic polymerization).

In conclusion, one possible solution to this dilemma would be the use of sufficiently large colloid templates, resulting in accordingly large and mechanically stable pore walls. Such materials were already described as three-dimensional ordered macroporous (3DOM) materials, which are of potential importance in catalysis, selective separation, sensor arrays, miniaturized electronic and magnetic devices, and communications with optical band gaps [13, 14]. Many studies on the synthesis of 3DOM materials have been reported, utilizing poly (styrene) (PS) and poly (methyl methacrylate) (PMMA) colloidal crystal templating routes for macroporous inorganic oxides [15, 16], metals and alloys [17], and sulfated zirconia [18]. However, to the best of our knowledge, there are no reports on porous CeO_2 possessing three-dimensional ordered inverse opal structure with a well-defined macropore structure with pores in the range below 200 nm. Since a 3DOM ceria would show a quite low surface area, the main scope of the present study was the generation of sufficiently small polymer colloids to obtain relatively small macropores and, putting this strategy to its limits, even mesopores with pores being significantly smaller than 100 nm. For this purpose, we chose PMMA colloid particles as templates, which are advantageous over PS templates because of better wettability with polar solvents (such as H_2O and alcohol), milder removal conditions, and also they introduce fewer structural defects [17]. In the synthesis of PMMA latex spheres templates, the emulsifier-free emulsion polymerization technique was employed and extended according to literature [19]. Depending on the ratios of the reactants, sphere diameters in various batches ranged from 320 to 90 nm, which were then used to generate porous replicas of crystalline cerium oxide. Furthermore, the colloid particle size could be further reduced by adding a surfactant during the polymerization. It will be demonstrated that 3DOM structures of crystalline ceria can be obtained with a facile process by using PMMA colloidal crystal templates, achieving even pore sizes down to ca. 30–40 nm. The sizes and close-packed structure of PMMA latex spheres were studied in detail depending on the concentration of added SDS. Scanning electron microscopy (SEM), transmission electron microscopy (TEM), X-ray diffraction (XRD), Hg porosimetry, and N_2 sorption were employed to study the properties and structure of the macro-and large mesostructured CeO_2 materials. The XRD data of the meso- and macroporous CeO_2, calcined at different temperatures, were analyzed by Rietveld refinements to study in detail the dependence of the crystallite size upon the heat-treatment temperature. Thereby, our study aimed at a better general understanding of the crystallization behavior of sol–gel derived CeO_2 within meso- and macroporous framework.

Experimental section

The surfactant-free PMMA latex spheres were prepared by emulsion polymerization of methyl methacrylate monomer (MMA) in the presence of potassium peroxodisulfate initiator in deionized water at 70 °C for 2 h according to literature [19]. Before polymerization, the monomer (MMA) solution was bubbled by nitrogen for 20 min under stirring to deactivate the inhibitors. To decrease the particle size of PMMA, sodium dodecyl sulfate (SDS) was used as surfactant. The close-packed colloidal crystal

templates were obtained by centrifugation. The synthesis conditions for specific samples are listed in Table 1.

In a typical synthesis of porous CeO_2 materials, 1.86 g of $CeCl_3 \cdot 7H_2O$ (Aldrich) was mixed with 10 ml of ethanol under mild stirring. After homogenization of the mixture solution (0.5 mol/l), appropriate amount of closed-packed PMMA colloidal crystals templates were deposited on a filter paper in a Buchner funnel under vacuum and soaked with ethanol. The precursor solution of $CeCl_3 \cdot 7H_2O$ was added drop wise to cover the latex spheres completely while suction was applied followed a reported route [15]. After drying the composite in a vacuum oven at 60 °C for 30 min, the composites were soaked in ammonia solution (2 mol/l) for 3–5 min and dried in a vacuum oven over night. The PMMA templates were removed by calcination in flowing air keeping at 310 °C for 3 h, and then at 450 °C, 550 °C for 4 h, respectively, (heating rate, 2 °C/min).

Scanning electron microscopy (SEM) images were performed on a Zeiss DSM 940. Transmission electron microscopy (TEM) images with high contrast were obtained using a Zeiss EM 912Ω at an acceleration voltage of 120 kV. Samples were ground in a ball-mill and dispersed in ethanol. One droplet of the suspension was applied to a 400-mesh carbon-coated copper grid and left to dry in air. The wide angle X-ray diffraction (XDR) measurements in reflection were performed using a D8 diffractometer from Bruker instruments (wavelength 0.154 nm). Hg-porosimetry experiments were performed with a Mercury porosimeter Pascal 440 (CE instruments). Nitrogen sorption experiments were conducted using a Micromeritics Tristar 3000 automated gas adsorption analyzer. Samples were degassed at 100 °C in a Micromeritics VacPrep061 degasser overnight before sorption measurements.

Rietveld refinement

The Rietveld refinement was performed using the program FULLPROF [20]. The crystal structure was refined in the space group of CeO_2, *Fm*-3*m* (225). The background was taken to be the polynomial function of 2θ of the 3rd order, because only in this case was the best background modelling obtained. The proper choice of profile function is very important if one wants to make size-microstrain analysis. In our case, we made the assumption that the profile broadening due to the grain size effect can be modelled with Lorentzian function, and broadening due to the microstrain can be modelled with Gaussian function. Therefore, the diffraction profile function was chosen to be the modified Thompson–Cox–Hastings pseudo-Voigt (T–C–H pV), which is linear combination of Lorentzian and Gaussian function [21]. The choice of this profile function makes the size-microstrain analysis straightforward. The instrumental contribution to the peak broadening was removed by the deconvolution method. To do that, we used the crystalline standard α-Al_2O_3 whose diffraction pattern was recorded under the same condition as those of investigated samples. The line broadening of α-Al_2O_3 XRD pattern is due to the instrumental broadening only, which is always included in XRD measurement due to the imperfections of the diffractometer (aberration, divergence, etc.).

The atomic fractional coordinates were kept constant in refinement procedure. Instrumental profile asymmetry was modelled using asymmetry correction functions with two refinable parameters for 2θ angles lower than 40 °. The quality of Rietveld refinement was evaluated in terms of the discrepancy factor (weighted residual error), R_{wp}, and the goodness-of-fit indicator, GoF.

Results and discussion

Structure of closed-packed PMMA latex spheres templates

Figure 1 shows SEM images of the colloidal crystals of PMMA with various particle sizes and well-defined ordered closed-packed arrays in three dimensions (3D). The diameter of the surfactant-free PMMA latex spheres (Fig. 1a) was ca. 300–320 nm, also showing that the diameters of the spheres were narrowly distributed. The morphology of latex spheres was well-defined, possessing a close-packed arrangement over a range of hundreds of micrometers, which is similar to reported findings for polystyrene spheres (PS) templates [15, 22, 23]. In the absence of surfactant, the latex sphere sizes of PMMA were partially decreased with increasing initiator concentration and reducing the concentration of monomer [19]. To reduce the size of PMMA latex spheres more significantly, SDS was used as a surfactant, which provides further dispersion of the monomer while more growing beads are produced (see Table 1). Figure 1b and c depict SEM images of the PMMA latex spheres of 170–190 and

Table 1 Synthesis conditions for PMMA colloidal crystals templates

	Surfactant	Monomer	Initiator	Average diameter of PMMA (nm)
Sample	SDS (mol/l)	MMA (mol/l)	$K_2S_2O_8$ (mol/l)	
PMMA 1		0.895	5.0×10^{-4}	300~320
PMMA 2	1.7×10^{-4}	0.688	2.1×10^{-3}	170~190
PMMA 3	8.5×10^{-4}	0.688	2.1×10^{-3}	90~100

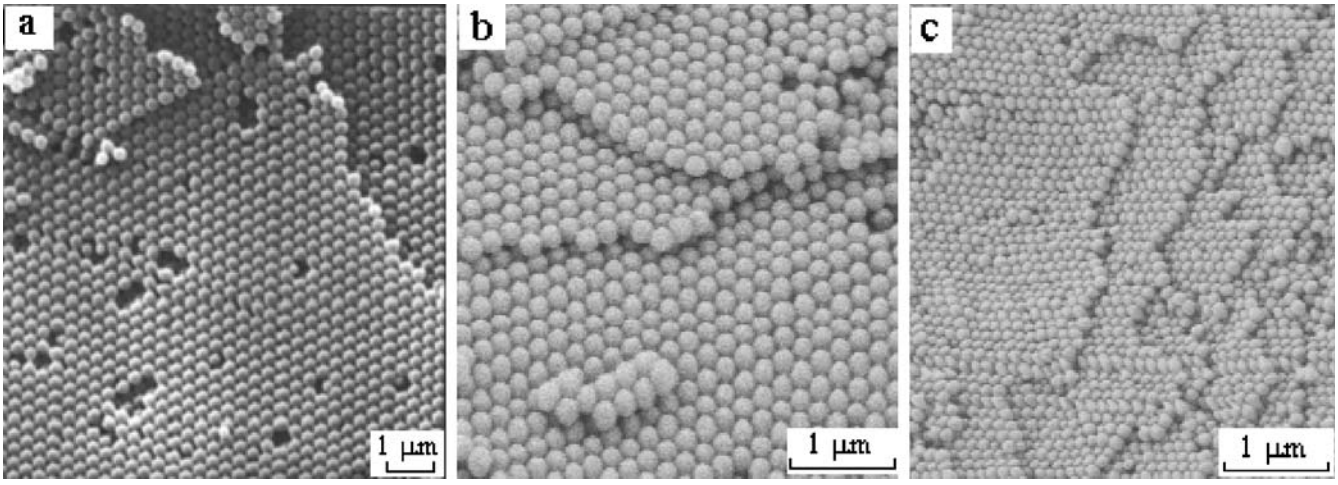

Fig. 1 SEM images of centrifuged PMMA colloidal crystal templates synthesized at different concentration of surfactant SDS: **a** surfactant-free; **b** 1.7×10^{-4}; and **c** 8.5×10^{-4} mol/l

90–100 nm in diameter, corresponding to 1.7×10^{-4} and 8.5×10^{-4} mol/l of SDS concentration, respectively. It is important to note that the sizes of PMMA spheres were significantly decreased with increasing the concentration of SDS, and they remained well defined and ordered closed-packed arrays in three dimensions, even after centrifugation.

Macro- and large mesostructure

Macropores and large mesopores of CeO_2 were fabricated by using the PMMA colloidal crystal templates with various bead sizes. Figure 2a presents the SEM image of the macroporous CeO_2 structure after calcination at 450 °C. It is seen that the removal of PMMA templates does not destroy the original ordered structure replicated into CeO_2 matrix. The interconnected network of pores left in CeO_2 was still arranged in a well-ordered close-packed structure. An average pore diameter of 200–240 nm was obtained with 300–320 nm PMMA sphere templates, providing a wall thickness of about 45–60 nm. The pore size was typically 30% smaller than that of the PMMA spheres due to shrinkage during calcination. Table 2 lists structural parameters of 3D macro- and large mesoporous CeO_2 treated at 450 °C. CeO_2 with smaller closed-packed pores of 70–80 nm in diameter could be obtained with 170–190 nm PMMA sphere templates (Fig. 2b). The extent of pore shrinkage increased to 58% (compared to the initial PMMA spheres used). Accordingly, the wall thickness decreased to of 30–35 nm, and the spherical pores were interconnected through windows to form the 3DOM structure. Hence, this material can already be regarded as a framework of large mesopores. More importantly, the usage of even smaller colloid particles allowed to generate

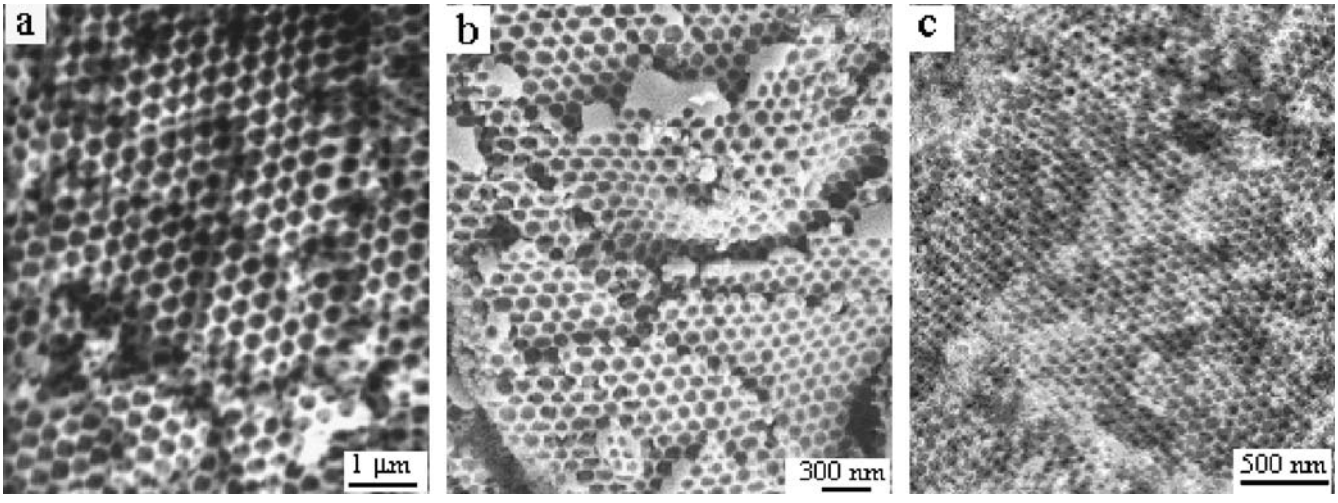

Fig. 2 SEM images of calcined pore CeO_2 materials with **a** 200–240 nm macrostructure; **b** 70–80 nm small macrostructure; and **c** 30–40 nm large mesostructure

Table 2 Structural parameters of 3D macro- and large mesoporous CeO_2 treated at 450 °C

Sample	Average diameter of PMMA spheres (nm)	Average pore void diameter (nm)	Linear shrinkage (%)	Thickness of walls (nm)	BET surface area (m^2/g)
CeO_2(1)	300~320	200~240	29	45~60	21
CeO_2(2)	170~190	70~80	58.3	30~35	46
CeO_2(3)	90~100	30~40	63.2	20~30	100

pores of only 30–40 nm, starting from 90–100 nm PMMA spheres (Fig. 2c), and pore shrinkage is 63%. The extent of shrinkage increased with decreasing the sizes of PMMA latex spheres, because for smaller beads, it is difficult to resist intensive shrinkage of crystallization in the walls. The TEM images, as shown in Fig. 3a and b, further confirm that the pore size of the large mesoporous structure is 30–40 nm and the pore wall thickness is 20–30 nm. Hg-porosimetry investigation also revealed a pore size distribution that is centered at ca. 30–40 nm (Fig. 4). The distribution at higher particle dimensions was due to the interparticle cavities.

It is noteworthy that such a well-ordered mesopore structures could be obtained by straightforward precipitation of a cerium oxide precursor inside the PMMA colloidal crystals and subsequent calcination.

Annealing behavior

The removal of PMMA template by calcination and the crystallization of the walls into CeO_2 nanocrystals can have significant effects on the quality of the pore structure of the large mesostructured CeO_2 materials. As determined by thermogravimetric analysis [17], PMMA colloidal crystals start to lose weight abruptly at around 305 °C and are completely decomposed at about 370 °C in air, which is lower than the decomposition temperature of PS colloidal crystals (380–460 °C). From this point of view, PMMA is a better template for the synthesis of mesostructured, crystalline CeO_2, because it can be removed at lower temperature, which prevents extensive crystal growth. To keep the large mesostructure intact, a slow heating rate (2 °C/min) and thermal treatment process keeping at 310 °C for 3 h were employed to ensure a gentle calcination process and complete removal of the PMMA template, leading to products with a lower carbon content at a given calcination temperature.

By contrast, in previous synthesizes of mesoporous CeO_2, using molecular surfactant templates, the removal of templates and the crystallization were usually carried out at high temperature (450–550 °C) and often accompanied by collapse of the mesoporous structure [7, 8]. It is evident that large primary wall grains can destroy the mesostructure, if such a process starts in much thinner ceria walls. As

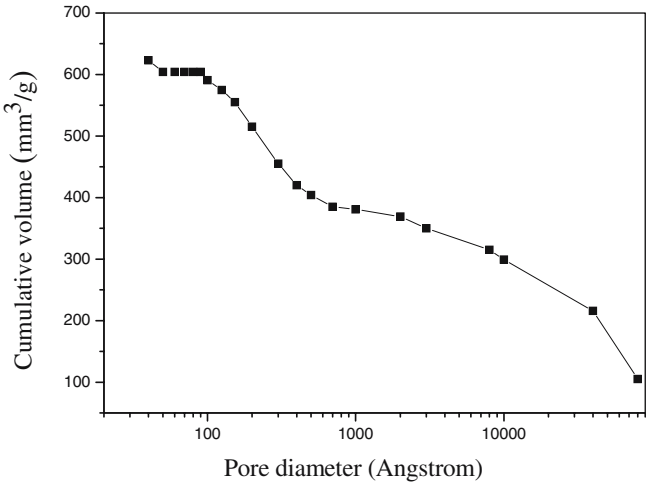

Fig. 4 Pore size distribution of the sample (CeO_2) obtained from Hg porosimetry

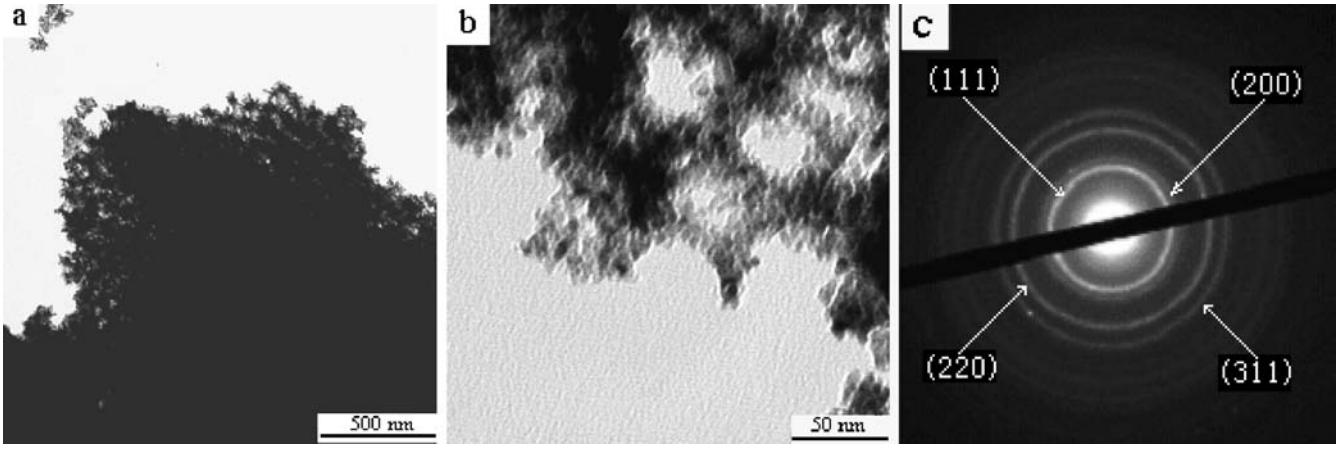

Fig. 3 TEM images of the large mesostructured CeO_2 materials calcined at 450 °C with different magnification **a** and **b**; selected area electron diffraction of the same sample (**c**)

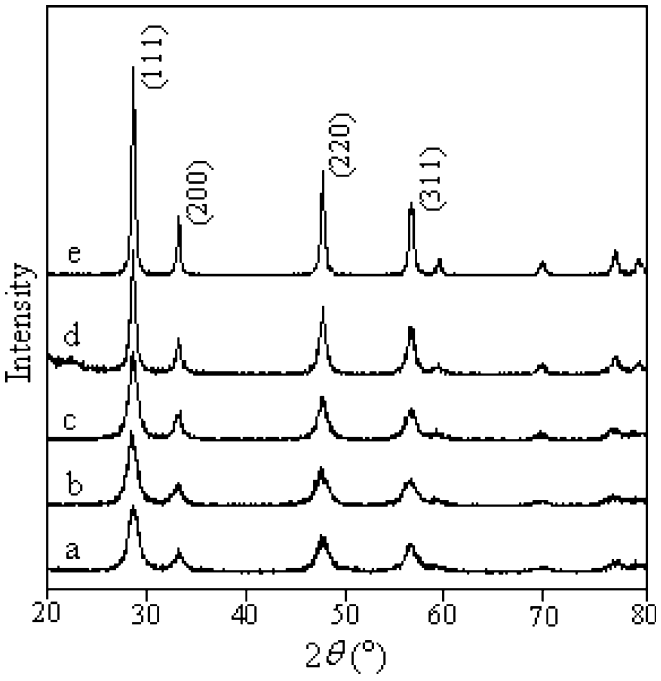

Fig. 5 XRD diffractograms of the large mesostructured CeO_2 materials calcined at different temperature: **a** 350 °C; **b** 450 °C; **c** 550 °C; **d** 650 °C; and **e** 750 °C

one of the major advantages, the PMMA colloidal crystal template shows stronger resistance to growth of nanocrystals because of its "hard beads" property and thick walls (ca. 20–30 nm). Therefore, the preparation of the large mesostructured CeO_2 from colloids requires a less precise control of the heat treatment and crystallization process.

By XRD characterization, the phases of the crystalline components in the large mesostructured CeO_2 samples could be identified as a single phase of a cubic fluorite structure, which is consistent with the phase determined by selected area electron diffraction (SAED) (Fig. 3c) of an ordered area in the TEM treated at 450 °C. The SAED displays diffraction rings characteristic of a structure composed of little domains with crystallographic axis randomly oriented with respect to each other. The *d*-spacings measured from the diffraction rings are in agreement with the face-centered cubic cerianite structure (ICDD PDF04-0593), proving its high crystallinity.

To obtain further insights into the crystallization behavior, temperature-dependent XRD measurements (Fig. 5) were performed on the sample with 30–40 nm pores ("large mesostructured" CeO_2). The XRD data revealed that already at 350 °C (Fig. 5a), a certain pronounced degree of crystallinity was present. However, the mesostructure with thicker walls was only stable up to 550 °C (Fig. 6), owing to extensive growth of nanocrystals. The large mesostructured CeO_2 calcined at 550 °C seems to represent a borderline where the CeO_2 crystallite and PMMA template size are still in a region that the mesostructure is maintained during the crystallization process. Larger

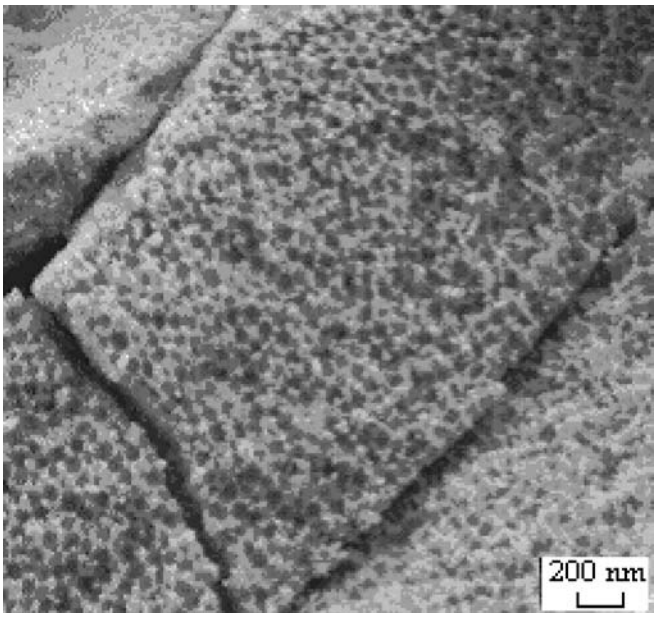

Fig. 6 SEM image of the large mesostructured CeO_2 materials calcined at 550 °C for 4 h

nanocrystals created at higher temperature destroy the present large mesopore structure.

To further elucidate the crystallization behavior of CeO_2 in mesopore frameworks, the structural and microstructural parameters were calculated using the Rietveld refinement of XRD powder patterns. The selected XRD pattern, together with the corresponding Rietveld refinement plot for the large-mesoporous CeO_2 calcined at 350 °C, is shown in Fig. 7. Closer inspection of the difference curve shows a good agreement between experimental and calculated diffraction profile and confirms validity of the structural model.

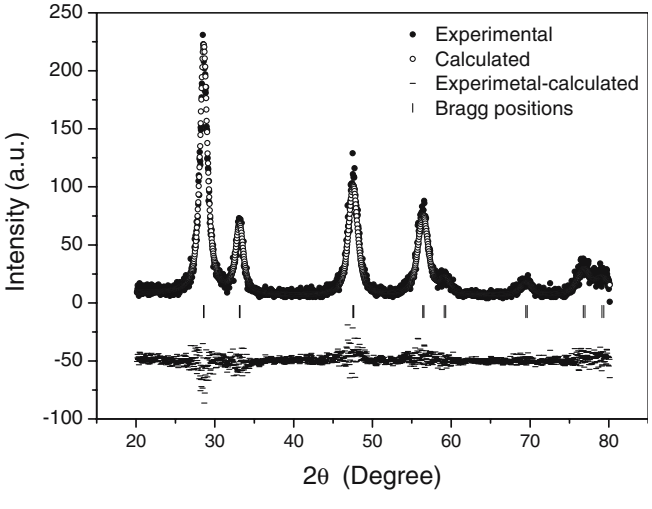

Fig. 7 Rietveld plot of CeO_2 calcined at 350 °C. The *thick marks* correspond to cubic phase

Ceria has the fluorite, CaF_2, structure, with 8-coordinate cations and 4-coordinate anions. It can be visualized as a cubic close-packed array of metal atoms with filling of oxygen all the tetrahedral holes; the structure-determining OCe_4 coordination tetrahedra thereby share all edges in three dimensions. The results of Rietveld refinement of ceria samples calcinated at different elevated temperatures are summarized in Table 3. Concerning lattice parameter, it can be seen that their values agree well with ICDD value, a_0=5.411 Å (ICDD PDF34-394). The slight changes of lattice parameter values with the increase of calcination temperature cannot be attributed to the real process because these changes are within their estimated standard deviations. However, the only exception is the sample calcinated at 750 °C, where this is not the case, and the unit cell parameter shows a slight contraction in comparison with all lower calcination temperatures. From the refined unit cell parameters and known values of fractional atomic coordinates of Ce and O atoms, the main interatomic distances were deduced. For instance, for the sample calcinated at 350 °C, the Ce–O bond length in coordination OCe_4 tetrahedron is 2.342(1) Å; the shortest Ce–Ce distance is 3.824(1) Å, and the shortest O–O interatomic distance is 2.704(1) Å (See supporting information in Table 4 in Appendix).

As a main benefit of the Rietveld refinement, the crystallization behavior could be accurately determined as a function of the annealing temperature. The extracted values of volume-weighted average grain (crystallite) size/average maximum microstrain of ceria samples showed a tendency of an increase with temperature. One notices that increasing the temperature from 350 to 750 °C causes significant grain growth, resulting in grain size increase from 6.2 to 20.9 nm. Simultaneously, the average maximum microstrain decreased in the same temperature range from 74.6×10^{-4} to 21.8×10^{-4}. The exception is the temperature of 550 °C, at which we observed a slight increase of average maximum microstrain from 46.3×10^{-4} (450 °C) to 53.2×10^{-4}. The microstrain is generally a measure of defects contained in crystal lattice. In most cases, the lattice defects are in the form of dislocations (line defects) and the incorporation of foreign ions (point defects) into the structure. The increase of calcination temperature caused the annihilation of dislocations, resulting in a decrease in the microstrain value. However, the observed increase of microstrain at 550 °C could be attributed to incorporation of impurities into the CeO_2 lattice. Probably at this temperature, the activation energy for impurities release is reached, resulting in their incorporation into the lattice and consequently increasing the microstrain.

Table 3 Structural data and refinement parameters for CeO_2 material calcined at different temperatures calculated by Rietveld refinement of XRD powder patterns

Temperature (°C)	Crystallite size (nm)	Unit-cell parameter (Å)	Crystallite microstrain (*e*) (%)
350	6.2	5.408 (2)	0.75
450	5.7	5.409 (2)	0.46
550	6.9	5.410 (1)	0.53
650	13.5	5.409 (1)	0.49
750	20.9	5.4054 (4)	0.22

Hence, the detailed XRD analysis helped to understand the distinct crystallization behavior of CeO_2 in mesopore structures: we found recently that in mesopore systems with ca. 15 nm in size the initial crystallite size (at ca. 250 °C) was only ca. 3 nm. However, in spite of the small nanocrystallite size, such materials usually undergo pore collapse upon heat treatment, starting even already at relatively moderate temperatures of 350 °C [9, 10]. Taking into account the present results, this sensitivity of CeO_2 mesostructures can be attributed to the significant growth of nanocrystals around 350–400 °C. Obviously, too small pore walls will not be able to sustain such excessive crystallization, while our present materials are stable enough with the pore walls being on the order of at least 30 nm.

Nitrogen sorption

The pore characteristics of the macroporous and large mesoporous CeO_2 were further characterized by N_2 physisorption (Fig. 8a). The shape of the isotherm (A) (Fig. 8a), obtained from macrostructured CeO_2 with average pore size of 200–240 nm, can be classified as a type II nitrogen adsorption isotherm with a BET surface area of only 20 m^2/g. The almost linear section of the isotherm suggests that the product is macroporous. However, the hysteresis loop is attributed to capillary condensation in a minor fraction of mesopores, which is similar to previous reported 3DOM NiO systems [24]. Curve (B) (Fig. 8a) was obtained from CeO_2 with average pore voids of 70–80 nm and corresponds to a transition between type II and IV isotherms, already indicating an evolvement from macroporous to mesoporous material, and the BET surface area rose to 46.12 m^2/g. A characteristic type-IV nitrogen adsorption isotherm [Fig. 8a isotherm (C)] was observed for the inverse opal large mesostructured CeO_2 with average pore voids of 30–40 nm, which is typical of a mesoporous material, giving rise to BET surface area of 100 m^2/g and an average pore size around 30 nm. The shape of the isotherm is in agreement with results from a CeO_2 system templated by small molecular precursors without long-range order structure [7]. We do not have a direct evidence to clarify that the hysteresis loop at high P/P_0 associated with capillary condensation taking place in mesopores can be attributed to the inverse opal large mesoporous structure. However, from the evolvement observed from curve (A) to the curve (C) in Fig. 8a and

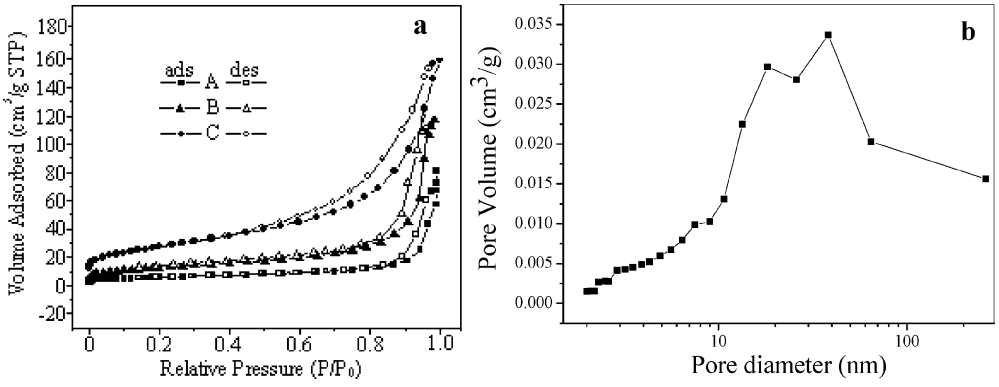

Fig. 8 **a** A representative N_2 adsorption/desorption isotherm for macro- and mesostructured ceria with different pore sizes: *A* 200–240 nm; *B* 70–80 mn; and *C* 30–40 nm calcined at 450 °C for 4 h. **b** The BJH pore size distribution of the large mesoporous CeO_2 sample (obtained from desorption branch of isotherm *C* in Fig. 8a)

increase in surface areas, we believe that the transformation of the shapes of isotherms is due to decrease of pore sizes from macropores to mesopores, and is not due to textural mesopores existing within the wall structure, which is in accordance with result from SEM (Fig. 2) and TEM (Fig. 3). The BJH pore size distribution is shown in Fig. 8b revealing a broad pore size distribution centered around 40 nm, similar to the result obtained from Hg porosimetry (Fig. 4). However, it should be emphasized that the formal BJH pore size distribution does not give exact information because currently available sorption models are not applicable to such large mesopores.

Conclusions

This work describes the fabrication of macro- and large mesostructured CeO_2 with inverse opal structure by using PMMA sphere templates of various sizes and a straightforward thermal treatment processes. Through the addition of surfactant of SDS in the synthesis, the latex diameters could be tuned and also remarkably decreased down to 90 nm. These PMMA colloidal crystals were small enough to result in large mesoporous, crystalline CeO_2 (e.g., 30–40 nm) in pore size after calcination. Compared to mesoporous CeO_2 obtained from surfactants or block copolymers as templates, the inverse opal structure was thermally more stable, maintaining the mesoporous structure even during the crystallization of CeO_2. A further reduction of the colloid particle size was not possible by the emulsion polymerization technique used. The minimal pore size of the large mesopore is about 30–40 nm with a crystalline wall thickness of 20–30 nm. After the removal of PMMA template, the large mesostructured CeO_2 framework could be kept intact up to 450–550 °C and exhibited a high surface area of 100 m^2/g.

A detailed XRD study on the crystallization behavior of CeO_2 within the pore walls, applying the Rietveld formalism, revealed a significant increase in crystallite size at ca. 600 °C. However, this analysis also indicated that the nanocrystallite size (ca. 6–7 nm) obtained at moderate temperatures (350–400 °C) requires sufficiently thick pore walls to avoid damage to the pore architecture. Thereby, the XRD analysis points to a plausible explanation to the difficulties in the preparation of mesopores of <15 nm, which is usually performed using surfactant templates: the mechanical stability of such smaller mesostructures is not sufficient to compensate the mechanical stresses upon the continuous crystallization of CeO_2, and the pore walls are simply too thin to adjust the growth. Furthermore, the remarkable degree of shrinkage of ca. 50% can be regarded as a further aspect aggravating the synthesis of mesoporous CeO_2 by surfactant templating strategies because even an initially large mesopore size (ca. 20 nm using block copolymers) will be massively reduced and eventually collapse. It is worthy to note that our study also demonstrated that probably changes in the crystal structure (release of strain, etc.) occur at higher temperature (550 °C), which may also aggravate thin pore wall. In essence, the use of colloids opens a possibility to obtain mesoporous CeO_2 with relatively high surface area and porosity, using a low-cost procedure, and avoiding the usual difficulties in the synthesis based on surfactant templates. These materials can be considered promising for applications, because the preparation itself serves as a facile method for fabrication of large mesoporous materials and can be extended to prepare other large mesoporous metal-oxides with functionalities.

Acknowledgements The Max-Planck Society is thanked for financial support and Tongwen Wang acknowledges the National Natural Science Foundation of China (20163002) and Natural Science Foundation of Yunnan Province/China (2003E0005Z) for financial supports.

Appendix

Supporting Information

Table 4 Inter atomic distances extracted from structural data for different temperatures of calcination

Temperature (°C)	350	450	550	650	750
Ce-Ce (Å)	3.824(1)	3.825(1)	3.825(1)	3.825(1)	3.822(1)
Ce-O (Å)	2.342(1)	2.342(1)	2.343(3)	2.342(1)	2.341(1)
O-O (longer) (Å)	3.824(1)	3.825(1)	3.825(1)	3.825(1)	3.822(1)
O-O (shorter) (Å)	2.704(1)	2.705(1)	2.705(2)	2.704(2)	2.703(1)

References

1. Trovarelli A (1996) Catal Rev Sci Eng 38:439
2. Trovarelli A, de Leitenburg C, Boaro M, Dolcetti G (1999) Catal Today 50:353
3. Kaspar J, Fornasiero P, Hickey N (2003) Catal Today 77:419
4. Kaspar J, Fornasiero P (2003) J Solid State Chem 171: 9
5. Steele BCH (2000) Solid State Ion 129:95
6. Murray EP, Tsai T, Barnett SA (1999) Nature 400:649
7. Terribile D, Trovarelli A, Llorca J, De Leitenburg C, Dolcetti G (1998) J Catal 178:299
8. Lyons DM, Ryan KM, Morris MA (2002) J Mater Chem 12: 1207
9. Brezesinski T, Antonietti M, Groenewolt M, Pinna N, Smarsly B (2005) New J Chem 1:237
10. Brezesinski T, Erpen C, Iimura KI, Smarsly B (2005) Chem Mater 17:1683
11. Corma A, Atienzar P, Garcia H, Chang-Ching JY (2004) Nat Mater 3:394
12. Desphande AS, Pinna N, Smarsly B, Antonietti M, Niederberger M (2005) Small 1:313
13. Wijnhoven JEGJ, Vos WL (1998) Science 281:802
14. Blanford CF, Schroden RC, Al-Daous MA, Stein A (2001) Adv Mater 13:26
15. Holland BT, Blanford CF, Do T, Stein A (1999) Chem Mater 11:795
16. Yan H, Blanford CF, Holland BT, Smyrl WH, Stein A (2000) Chem Mater 12:1134
17. Yan H, Blanford CF, Lytle JC, Carter B, Smyrl WH, Stein A (2001) Chem Mater 13:4314
18. Al-Daous MA, Stein A (2003) Chem Mater 15:2638
19. Zou D, Ma S, Guan R, Park M, Sun L, Aklonis JJ, Salovey R (1992) J Polym Sci A Polym Chem 30:137
20. Rodriguez-Carvajal J (2000) FULL-PROF—a program for Rietveld Refinement, Laboratorie Leon Brillouin, CEA-Saclay, France
21. Thompson P, Cox DE, Hastings JB (1987) J Appl Crystallogr 20:79
22. Kuang DB, Brezesinski T, Smarsly B (2004) J Am Chem Soc 126:10534
23. Zhou Y, Antonietti M (2003) Adv Mater 15:1452
24. Yan H, Blanford CF, Holland BT, Smyrl WH, Stein A (2000) Chem Mater 12:1134